New Folder Name Final Draft - Suspension Paper

Bob -

Enclosed is a copy of the final draft of our suspension paper. Please pass it on to anyone at CalTech who wants to look at it. It's about 20% shorter than the previous draft; we've also cut out four figures. We added some discussion of the position sensors (which includes a new figure) and added Joe Kovalik as an author.

Thanks again for your comments.

Michelle

Please read if interested, and pass along. (If you don't intend on reading it, please pass along without delay!)

- ☑ A. Abramovici
- ☑ R. Drever
- ☑ Y. Gursel
- ☑ F. Raab
- ☑ M. Zucker
- ☑ S. Kawamura
- ☐ C. Akutagawa (file)

A Double Pendulum Vibration Isolation System for a Laser Interferometric Gravitational Wave Antenna

M. Stephens[1], P. Saulson[1,2], J. Kovalik[1]

[1]Massachusetts Institute of Technology, 20F-001, 77 Massachusetts Ave., Cambridge, MA 02139

[2]Joint Institute for Laboratory Astrophysics, University of Colorado at Boulder, Campus Box 440, Boulder, CO 80309-0440

We have developed a nested double pendulum suspension system for the test masses of a laser interferometric gravitational wave antenna. The system consists of a mass hung as a pendulum inside a shell mass which is also hung as a pendulum. A set of two-degree-of-freedom reflective "shadow detectors" senses motion of the shell relative to ground. Identical sensors measure motion of the mass relative to the shell.

The equations of motion were solved to find the resonances and mode shapes for all of the rigid body degrees of freedom. The predicted resonant frequencies agree well with the measured frequencies. A damping system has been implemented that damps the resonances by applying forces to the shell mass alone.

The vibration transfer function along the optic axis was measured. It shows the steep f^{-4} decline expected of a double pendulum. We have also measured the vertical vibration transfer function and the cross coupling due to misalignment.

A set of plates on the inner surface of the shell allows the application of low

noise electrostatic forces directly to the test mass for high-bandwidth control such as interferometer fringe lock. We have measured the response of the system to this input, and compared it to that predicted by our model equations of motion. We have determined that there exist stable feedback loops that can maintain fringe lock.

The possibilities of active isolation are discussed.

I. Introduction

Interferometric gravitational wave detectors measure extremely small relative displacements between the mirrored faces of several "test masses" arranged in the L-shaped configuration of a Michelson interferometer[1]. The design of the test mass suspensions must satisfy several demands simultaneously. Firstly, the test masses must be approximately free in a frequency range of interest so that they can respond to the weak gravitational forces in a gravitational wave. Secondly, they must be free from mechanical noise which might mask the tiny motions expected from a gravitational wave. Finally, they must be controlled so the interferometric read-out system can be aligned and held locked to a fringe.

The first requirement, dynamical response approximately that of a free mass, can be satisfied by supporting the test masses with some form of compliant connection to the outside world. At low frequencies, the response of the test mass is dominated by the spring constant of its mounting. But above the resonant frequency of the oscillator, the response approaches that of a free mass.

The compliant mounting of the test mass is a start toward satisfying the second requirement as well. One of the largest sources of mechanical noise is the ubiquitous background of seismic noise communicated to the test masses through their supports. The compliant suspension functions as a vibration isolator, attenuating the external vibrations at frequencies high compared to the resonance. If the isolation provided by one oscillator (proportional to $\left(\frac{f}{f_0}\right)^2$ where f_0 is the

resonant frequency of the oscillator) is insufficient, it can be supplemented by additional mass-spring stages.

Noise can also be generated within the structure itself. The most fundamental mechanism of this type is thermal noise, the analogue of Brownian motion in the macroscopic suspension. The amplitude of this noise is minimized by arranging for the lowest possible level of mechanical losses in the final stage of the suspension. A pendulum is almost always used for the suspension of the mass itself, because of its low losses.

There are several different control functions to be performed. The low mechanical losses used to reduce thermal noise have as their side effect high-Q resonances. Servo damping is used to reduce the mechanical excitation of these modes. In addition, control forces must be applied to the compliantly-mounted test mass to keep it aligned with the rest of the optical system, and to adjust the optical path length to fix the relative phase of the interfering light beams in the interferometer. All of these functions must be performed without short-circuiting the vibration isolation of the system, and without introducing significant amounts of mechanical noise.

A number of approaches to meeting these demands have been taken by workers in the field [2, 3, 4, 5, 6]. In this paper, we describe a suspension system that we designed with the goal of meeting the stringent specifications necessary to detect and study gravitational waves from expected astrophysical sources with

a detector such as the long-baseline interferometers being developed by the Caltech/MIT LIGO project and several groups around the world.

In the next section, we explain the specific design requirements we set for the suspension, showing how this led to a system with the features that we adopted. The succeeding sections describe an extensive series of tests that we performed to try to determine how well the suspension performed. Finally, we describe what aspects of the performance still need verification.

II. Design Principles

A central theme of the design was to keep the structure of the test mass itself as simple as possible. This was done in an attempt to maintain the high mechanical Q of the test mass and thus minimize the thermal excitation of the internal resonances of the test mass. We strove to find alternatives to control mechanisms that involve attachment of magnets for actuators or shadow tabs for position sensors. This is the reason for the choice of electrostatic actuators for the forces that need to be applied to the test mass itself. The pendulum is hung by a single loop of wire around its middle, as done by the Max Planck group[5]. For applications that require direct sensing of the position of the test mass, we made provision for reflective optical sensors.

Another theme of the design was to attempt to achieve sufficient isolation so that gravitational wave interferometers could be limited by the fundamental measurement noise, photon shot noise, down to a frequency of 100 Hz. We

wanted to do this without the use of elastomer-based isolation stacks [7, 8] or air-spring systems [9], believing that a simpler system would suffice. This does not preclude the use of other isolators with this system.

The solution we adopted to meet these requirements is the nested double pendulum. The vibration transfer function should be that of two low-frequency oscillators in series, $\frac{f_{0_1}^2 f_{0_2}^2}{f^4}$ in the limit of high frequencies where f_{0_1} and f_{0_2} are the resonant frequencies of the two-oscillator system. By nesting the test mass inside the closely-fitted shell mass, we provided a platform from which to apply the control forces. This platform is itself vibration-isolated by virtue of its placement on the upper mass of the double pendulum, although it is not as quiet as the test mass itself. (An alternative design based on similar ideas has been pursued by Cantley et al. [4]).

This design offers the additional benefit that measurement of the relative displacement of the test mass with respect to the shell mass gives an error signal that can be nulled by a servo system that applies appropriate forces to the shell. This is the classic configuration for active vibration isolation, which effectively reduces the frequency of one of the normal modes of the isolation system (see refs.). Although we did not test the system in this style of operation, we studied some of the relevant transfer functions to learn its possibilities and limitations.

As a final design principle, we attempted to minimize the use of materials whose outgassing could interfere with the need to achieve a good vacuum in the

gravitational wave interferometer.

III. System Description

The nested double pendulum consists of a shell mass surrounding a 10 kg mirror mass. The mirror mass is a 20.32 cm diameter, 10.16 cm long cylinder. This aspect ratio was chosen so that the frequencies of the lowest orders of the vibrational modes of the cylinder are as high as possible [10, 11]. In this prototype, the mirror mass was made of aluminum. For an actual test mass in a full scale gravitational wave detector it most likely would be a quartz mirror.

The mirror mass is held about the middle by a single .2 mm diameter tungsten wire. The wire is close to breaking; thus, the violin mode of the wire is at the highest possible frequency. Two 0.32 cm diameter cylinders at ten degrees above the midline increase the normal force of the wire on the mirror mass at the point where the wire leaves the mirror mass to prevent slippage. The cylinders are held in place by friction.

The mirror mass has four polished flats on it that are used in conjunction with the reflective position sensors to measure motion of the mirror mass relative to the shell.

The 10 kg aluminum shell has a 25.4 cm outer diameter and is 18 cm long. The mirror mass hangs centered within the shell with a 1 mm gap on all sides between the inner edge of the shell and the mirror mass. Clamps on the top of the shell hold the two ends of the tungsten wire that suspends the mirror mass.

To allow for the electrostatic actuators mentioned in the previous discussion, annuli at the front and back of the shell overlap the front and back of the mirror mass by 1.27 cm. The shell is cut into sections that are insulated from each other by thin teflon sheets. Thus a voltage applied to the front and back plates can produce a force on the electrically grounded mirror mass. Both the front and the back overlapping sections of the shell are cut into four quadrants, allowing an axial force and two torques to be applied to the mirror mass from the shell.

The shell also has four holes drilled in it that allow mounting of reflective position sensors. These sensors are attached to the shell and, by using the reflective surfaces on the mirror mass, they measure motion of the mirror mass relative to the shell. Four position sensors attached to the ground use four reflective surfaces on the shell to measure motion of the shell relative to the ground.

The sensors consist of shadow detectors, which use a small infrared LED shining through a hole in the center of a quadrant photodiode. The light shines through the hole onto a polished flat on the shell mass that has a small dark patch in the center. The difference in the photocurrents from two opposite quadrants indicates the relative displacement of the sensor and the shell mass (Figure 1). The sensitivity is limited by shot noise down to frequencies below 5 Hz, at a level of $4 \times 10^{-10} \frac{m}{\sqrt{Hz}}$. This signal is linear over approximately 2 mm.

Attached to the shell are six magnets that are used by magnetic actuators. A 750 turn coil wound on a teflon core is attached to the ground near each magnet,

allowing adjustment of the position of the shell relative to the ground (a variant on a design developed by the Max Planck group[5]). The magnets are placed so that all six degrees of freedom of the shell can be controlled. The actuators produce an maximum force of about .03 N over a range of 1 mm.

The shell itself is hung as a pendulum. Four tungsten wires (also .2 mm in diameter), each in series with a coil spring, hold the shell and mirror mass. The wires are clamped to the shell at ten degrees above the midline.

Figure 2 shows a diagram of the suspension and defines the coordinate system that will be used throughout this paper.

The linearized equations of motion for the double pendulum suspension can be derived by finding the Lagrangian for the coupled system and then writing down the Euler-Lagrange equations in the small angle approximation. This is simplified by recognizing that for a system with no misalignment, the motion can be describe by four combinations of coupled motion. These are translation along the optic axis and rotation about the y-axis, translation along the y-axis and rotation about the optic axis, translation along the vertical axis, and rotation about the vertical axis.

Once the Euler-Lagrange equations have been derived, the dynamics of the system are completely described. The equations of motion can be solved numerically, and the resonant frequencies and the eigenvectors of the rigid body normal modes are easily computed. A computer model was used to predict resonant fre-

quencies and transfer functions between pairs of drive and sensor signals. Table 1 presents a comparison of the rigid body resonant frequencies predicted by the model and the corresponding measured frequencies. The predicted frequencies agree closely with the measured frequencies. The largest error is in the prediction of the two highest frequencies, which are primarily due to the stretching of the tungsten wire that holds the mirror mass and is probably due to an error in the estimate of the spring constant of the tungsten wire.

IV. Damping

Because the suspension has low losses, the seismically driven motion of the mirror mass at the resonant frequencies is too large to allow a suspended optical cavity to remain in resonance. Therefore the rigid body motion at the resonant frequencies must be artificially damped. A damping system has been implemented in which a sensor detects motion of the shell mass at a position on the shell very close to the point at which the damping force is applied. Because the phase of the transfer function never goes through a phase shift greater than 180 degrees, independent of the number of resonances in the signal, the sensor signal is easily used as an error signal in a feedback loop. Figure 3 shows a typical open loop transfer function. The phase characteristics are similar for all of the loops.

For the double pendulum suspension, damping of the 10 lowest resonant frequencies in vacuum has been achieved with four independent damping loops. Two loops are needed to damp the four resonances that couple translation along

the optic axis with rotation about the y-axis. Two more loops are needed to damp the six other resonances. Figure 4 compares the power spectrum measured with the damping loops open and closed as measured by a position sensor that was not used in any of the damping loops.

By damping the motion of the suspension using forces applied only to the first pendulum stage, one can take advantage of the filtering of electronic noise by the second pendulum stage. The position sensors sense motion of the outer shell relative to the ground, and the magnetic pushers push on the shell from the ground. Pushing on the shell alone damps the motion of both the shell and the mirror mass because the motions of both masses at the resonant frequencies are strongly coupled. With noise from the coil driver electronics at $1.2 \times 10^{-10} \frac{N}{\sqrt{Hz}}$, a low closed-loop gain results in a controller induced position noise at the inner mass of $3 \times 10^{-19} \frac{m}{\sqrt{Hz}}$ at 100 Hz. The noise due to damping the mirror mass directly would be $\left(\frac{f}{f_o}\right)^2$ larger, or $2 \times 10^{-15} \frac{m}{\sqrt{Hz}}$ at 100 Hz. Any noise on the magnetic actuators due to fluctuating magnetic fields in the area is also filtered by $\left(\frac{f_0}{f}\right)^2$.

V. Isolation and cross-coupling

Isolation transfer functions along the optic axis and in the vertical direction were measured. Cross-coupling between vertical motion and optic axis motion and between motion along the y-axis and motion along the optic axis were also measured. All measurements were made in vacuum to prevent acoustic excitation

of the mirror mass.

To measure the isolation transfer function along the optic axis in vacuum an electromagnetic shaker was attached to the suspension point of the double pendulum via a bellows feedthrough. Accelerometers were placed along the optic axis of the mirror mass, the shell, and the suspension point. The shaker was used to shake the suspension point, and transfer functions between the shell and the suspension point and between the mirror mass and the suspension point were measured. To measure the cross-coupling between motion along the y-axis and the optic axis, the same shaker configuration was used but the suspension was turned 90° in the vacuum tank.

The shell transfer function along the optic axis follows the $\frac{1}{f^2}$ behavior expected for a single pendulum up to 113 Hz, where the internal resonances of the four coil springs dominate the transfer function (one could reduce the Q of the internal resonances with a passive magnetic damping scheme). The shell continues to isolate beyond these resonances, but the harmonics of the spring resonances at 339 Hz and the violin modes of the four wires holding the shell mass (at 430 Hz) begin to compromise the isolation (Figure 5). In addition, the inner mass transfer function follows the $\frac{1}{f^4}$ behavior expected for a double pendulum up to 113 Hz. It continues to isolate as $\frac{1}{f^2}$ with respect to the shell despite the internal spring resonances that compromise the shell's isolation. At 250 Hz an isolation of 160 dB was measured (Figure 6). The violin mode of the

two inner wires is expected at 1200 Hz; however, measurements of the isolation of the inner mass could not be made beyond 250 Hz because the suspension isolation was so effective that the measurements were dominated by electronic noise in the accelerometers.

The vertical isolation of the suspension and the vertical-to-optic-axis cross-coupling were also measured. There are two vertical resonances, one at 3.6 Hz due to the coil springs, and one at 26 Hz due to the stretching of the wire holding the mirror mass. The expected $\frac{1}{f^2}$ isolation of the mirror mass before the 26 Hz vertical resonance, and the $\frac{1}{f^4}$ isolation after this resonance was confirmed (Figure 7).

Figures 8 and 9 show the cross-coupling of y-axis motion to optic axis motion and the cross-coupling of vertical motion to optic axis motion. Figure 10 shows a composite of Figures 6, 7, 8, and 9 to demonstrate the actual optic axis isolation of the suspension system. It also includes the vertical isolation reduced by 65 dB, showing the contribution of vertical motion to the interferometer noise if the arms are 2/3 mrad away from level. (Arms that are 4 km long, if level at their midpoints, will depart from level at their ends by about 2/3 mrad because of the curvature of the earth.) It is apparent that for these tests the isolation of the suspension below 80 Hz is dominated by the vertical to horizontal cross-coupling. Above 80 Hz the cross-coupling is comparable to the optic axis isolation and does not seriously compromise the isolation.

An investigation into the cause of the cross-coupling indicates that the main contribution to the cross-coupling is misalignment at the take-off point of the single wire about the mirror mass. For example, if the loop of wire leaves the mirror mass at different points relative to the center of mass on each side the mirror mass will hang at a slight angle. If in addition the wire leaves the mirror mass at a slightly higher point on one side relative to the other, a vertical drive will cause a non-zero torque about the center of mass. This in turn will cause a rotation about the y–axis. Because the rotation point is by design above the center of mass, this rotation will cause a first order translation of the center of mass. The actual motions of the mirror mass caused by cross-coupling were more complicated than this, involving rotations about the vertical axis and the y-axis and translations along the optic axis and the y-axis.

These cross-coupling measurements should be taken to be "worst case" measurements since no special alignment tools were made to minimize misalignment during hanging.

VI. Fine Control

Fine control of the mirror mass is necessary to keep the interferometer fringe locked. This double pendulum suspension was designed so that the fine control could be done with high voltage actuators. By pushing on the mirror mass from the shell one can take advantage of the f^2 isolation of the shell to push from a quiet platform, thus reducing the amount of seismic noise transmitted to the mirror

mass through the actuators. By having high voltage plates on both the front and back of the electrically grounded mirror mass, an effective restoring force that is much smaller than any of the pendulum restoring forces can be obtained. This provides a forcer that does not interfere with the suspension isolation in addition to providing a force that is linear with respect to applied voltage.

The effective restoring force for small displacements of the mirror mass is calculated as:

$$\frac{dF}{dx}\Big|_{x_0} = \frac{A_{plate} V_{bias}^2}{\pi x_0^3} \qquad (1)$$

In this prototype suspension, the gap size $x_0 = .1$ cm, the bias voltage $V_{bias} = 1.33$ statvolts, is applied to both the front and the back plate, each plate section has an area $A_{plate} = 19$ cm^2 and the mass $m = 10^4$ gm. The effective resonant frequency due to this restoring is $f_0 = .165$ Hz. This effective frequency is much lower than any of the pendulum resonant frequencies, thus it has a negligible effect on the dynamics and isolation of the suspension.

With an input noise to the high voltage amplifiers of $2\frac{nV}{\sqrt{Hz}}$ and a gain of 50, the position noise at the mirror mass from the amplifier noise is $2 \times 10^{-19}\frac{m}{\sqrt{Hz}}$ at 100 Hz. This noise will be reduced by the loop gain in the interferometer locking servos.

Implementation of the fine control requires three servo loops, one to control translation of the mirror mass along the optic axis, one to control rotation about

the y-axis, and one to control rotation about the vertical axis. There must therefore be three stable loops. Not only must each individual loop be stable when closed, but all three loops must be closed at once without losing stability.

The first two of these loops interact because of the way the mirror mass is hung, with a single wire about the center. A force that translates the mirror mass along the optic axis couples to a rotation about the y-axis, and a force that rotates the mirror about the y-axis couples to a translation along the optic axis. By using normal coordinate transformations [12] the drives for these two coupled loops were optimized so that at frequencies much higher than the resonant frequencies this coupling was minimized. The Bode plots for each particular drive were calculated with the computer model. The two drives were then implemented on the prototype suspension. Each drive consisted of a combination of forces on the shell from the magnetic pushers and forces on the mirror mass from the high voltage pushers.

The rotation about the y-axis was measured with an optical lever, and the translation along the optic axis was measured with a capacitance transducer. Small differences in spacing between the front and back plates were compensated for by adjusting V_{bias} on one of the plates.

Figure 11 compares the measured and predicted transfer functions for the drive designed to optimize translation of the center of mass of the mirror mass while minimizing the coupling to rotation about the y-axis. Figure 12 compares the measured and predicted transfer function for the drive designed to optimize

rotation about the y-axis while minimizing the coupling to the translation of the center of mass of the mirror mass. These transfer functions have the proper phase characteristics needed for use in a stable feedback loop.

A servo system with both the translation loop and the y-axis rotation loop closed simultaneously was simulated on the computer. Stable operation is allowed. The point of this simulation was to demonstrate that both loops could be closed simultaneously while retaining stability; all of the detection circuitry was assumed to have an infinite bandwidth and the closed loop gain in this simulation could be chosen arbitrarily high.

VII. Active isolation

As mentioned in the introduction, we explored the possibilities of active isolation with this suspension. (For previous discussions of the topic, see [2,13]) The basic idea is to apply forces to the shell mass to null an error signal representing the relative displacement of the shell and the mirror mass. When the shell is accurately following the mirror mass (serving as an inertial proof mass), then it is transmitting less vibration than it would in the open-loop state. In the process, the servo loop has reduced the frequency of the gravest pendulation mode of the system.

Several aspects of the design will make it difficult to achieve much improvement in the seismic isolation from this suspension from active techniques. One problem is the coupling between rotation of the shell and translation of the mirror

mass. This is of a fundamentally different character than the coupling of the displacements of the centers of mass of the shell and the mirror. The relative displacement due to shell mass displacement vanishes in the limit of zero frequency, but a rotation of the shell causes a relative displacement of the centers of mass at zero frequency. This means that, unless the forces from the upper and lower actuators on the shell were precisely balanced, the low-frequency performance of an active isolation loop will always be limited by the rotations caused by the mismatch. This requirement could be alleviated if the suspension were redesigned so that the wire for the mirror mass left the shell at the point about which the shell rotates. Figure 13 demonstrates that there is a conditionally stable active isolation loop if one can perfectly balance the driving forces.

A second problem is perhaps more serious. As we have shown, the asymmetry in the isolation of the suspension is great enough that vertical vibration of the mirror is close to dominating the interferometer's response to seismic noise. This means that if we want to use active isolation to reduce the amount of seismic noise, we will need to improve the vertical isolation almost as much as the horizontal isolation. But the fact that the suspension is much stiffer in the vertical direction will substantially complicate implementation of a vertical active isolation loop. In particular, the signal-to-noise ratio for sensing vertical motion is greatly reduced because the relative motion between the shell and the mirror mass is small. The replacement of the relatively stiff tungsten wire holding the mirror mass with

a softer vertical isolator would improve the vertical isolation of the system and make it easier to actively isolate in the vertical direction if necessary.

For these reasons, we are not hopeful that this suspension's vibration isolation can be much improved by active isolation techniques although a few design changes could once again make this a candidate for active isolation. Another possibility for active isolation can be found in specially designed pre-filters from which the high-Q pendulum suspensions are hung[14].

VIII. Discussion

The results of our series of tests show this nested double pendulum to be a credible design for a test mass suspension in a high performance gravitational wave interferometer. The vibration isolation is consistent with the model. The damping servos perform well. The transfer functions for the fine control loops appear to have the required form. Active isolation remains a possibility, but would require some changes in the design.

Some aspects of the performance can only be fully tested when the suspension has been incorporated into a working interferometer. For example, tests with a sensitive interferometer would verify that the isolation we measured at large noise levels is obtained at ambient noise levels, and that there is no unexpected additive noise component.

Acknowledgments

We would like to thank Rai Weiss for extensive contributions. We would like

to thank Nelson Christensen for work on the high voltage amplifiers. We would also like to thank Ron Drever, Bob Spero, and Mike Zucker for useful discussions.

This work was supported by NSF grant PHY-8803557

References

[1]Thorne, K. S., in *300 Years of Gravitation*, edited by S. W. Hawking and W. Israel (Cambridge University Press, Cambridge, 1987), Chapter 9.

[2]Robertson, N. A., Drever, R., Kerr, I., Hough, J. Phys. E **15**, 1101 (1982).

[3]Del Fabbro, R., Di Virgilio, A., Giazotto, A., Kautzky, H., Montelatici, V., Passuello, D., Phys. Letters A **132** , 237 (1988).

[4]Cantley, C. A., Robertson, N. A., Hough, J. A., presented at 12th International Conference on General Relativity and Gravitation, Boulder, CO, 1989

[5]Shoemaker, D., Schilling, R., Schnupp, L., Winkler, W., Maischberger, K., Rudiger, A., Phys Rev D **38** no 2, 423 (1988).

[6]Linsay, P., Shoemaker, D., Rev. Sci. Instrum. **53**, No. 7, 1014 (1982).

[7] Drever, R. in *Gravitational Radiation*, edited by N. Deruelle and T. Piran (North-Holland Publishing Company, Amsterdam, 1983), pg. 330.

[8]Wolf, Ralph, Undergraduate Research Thesis, California Institute of Technology, 1987.

[9]Del Fabbro, R., Di Virgilio, A., Giazotto, A., Kautzky, H., Montelatici, V., Passuello, D., Rev. Sci. Instrum. **59**, 292 (1988).

[10]McMahon, G. W., J. Acous. Soc. Am., **36**, no1, 85 (1964).

[11]Hutchinson, J.R., J. App. Math., **47**, 901 (1980)

[12]Goldstein, H., *Classical Mechanics* , 2nd ed. (Addison–Wesley, Reading ,1980).

[13]Saulson, P. R., Rev Sci Instrum. **55**, 1315 (1984).

[14]Stebbins, R.T. Bender, P. L., Faller, J. E, Newell, D. B., Speake, C.C., , presented at 12th International Conference on General Relativity and Gravitation, Boulder, CO, 1989

Figure Captions

Figure 1a. An aligned shadow detector. The size of the absorbing patch is chosen so that no light falls on quadrant 1 or quadrant 2.

Figure 1b. The reflective surface has moved. Now more light falls on quadrant 1 than quadrant 2 so that the difference in the between the signals from the two quadrants is non-zero.

Figure 2. Nested double pendulum suspension system. The mirror mass has been drawn out of the shell to allow a better view of the hanging method used.

Figure 3a. A typical open loop transfer function for damping. This is the ratio of the voltage applied to the driver for the magnetic actuators to the voltage received from the appropriate position sensor.

Figure 3b. The same transfer function predicted by the computer model.

Figure 4. Power spectrum for the undamped and damped cases. The suspension is driven by the ambient seismic vibration.

Figure 5. Optic axis isolation of shell relative to the suspension point.

Figure 6.. Optic axis isolation of mirror mass relative to the suspension point.

Figure 7. Vertical isolation of the mirror mass relative to the suspension point.

Figure 8. Y-axis to optic axis cross-coupling.

Figure 9. Vertical axis to optic axis cross-coupling.

Figure 10. Composite optic axis isolation. The ground noise is assumed to be isotropic.

Figure 11a. Measured open loop transfer function for maximum translation drive. This is the ratio of the voltage received from the capacitance transducer to the voltage applied to the drive circuitry.

Figure 11b. Corresponding transfer function predicted by the computer model.

Figure 12a. Measured open loop transfer function for maximum tilt drive. This is the ratio of the voltage received from the optical lever to the voltage applied to the drive circuitry.

Figure 12b. Corresponding transfer function predicted by the computer model.

Figure 13. Predicted transfer function indicating a stable active isolation loop.

Predicted	Measured	Coupled Motions
.711 Hz	.690 Hz	translation along the y-axis and rotation about the optic axis
.800	.812	translation along the optic axis and rotation about the y-axis
.918	.920	rotation about the vertical axis
1.07	1.05	translation along the optic axis and rotation about the y-axis
1.22	1.22	translation along the optic axis and rotation about the y-axis
1.66	1.7	translation along the y-axis and rotation about the optic axis
2.05	1.9	rotation about the vertical axis
3.23	2.88	translation along the optic axis and rotation about the y-axis
3.57	3.63	translation along the vertical axis
4.75	4.84	translation along the y-axis and rotation about the optic axis
31.0	27.0	translation along the vertical axis
31.2	37.0	translation along the y-axis and rotation about the optic axis

Table 1. Predicted and measured rigid body resonances. The third column briefly describes the coupled motion for each resonance.

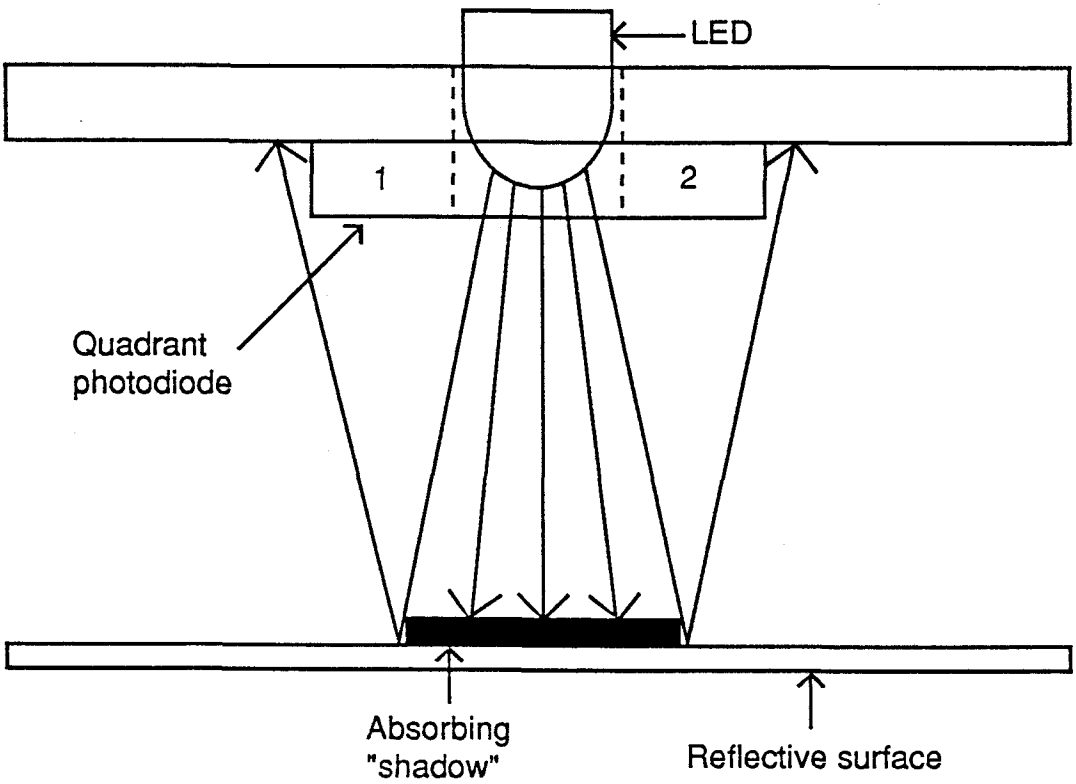
LED
1
2
Quadrant
photodiode
Absorbing
"shadow"
Reflective surface

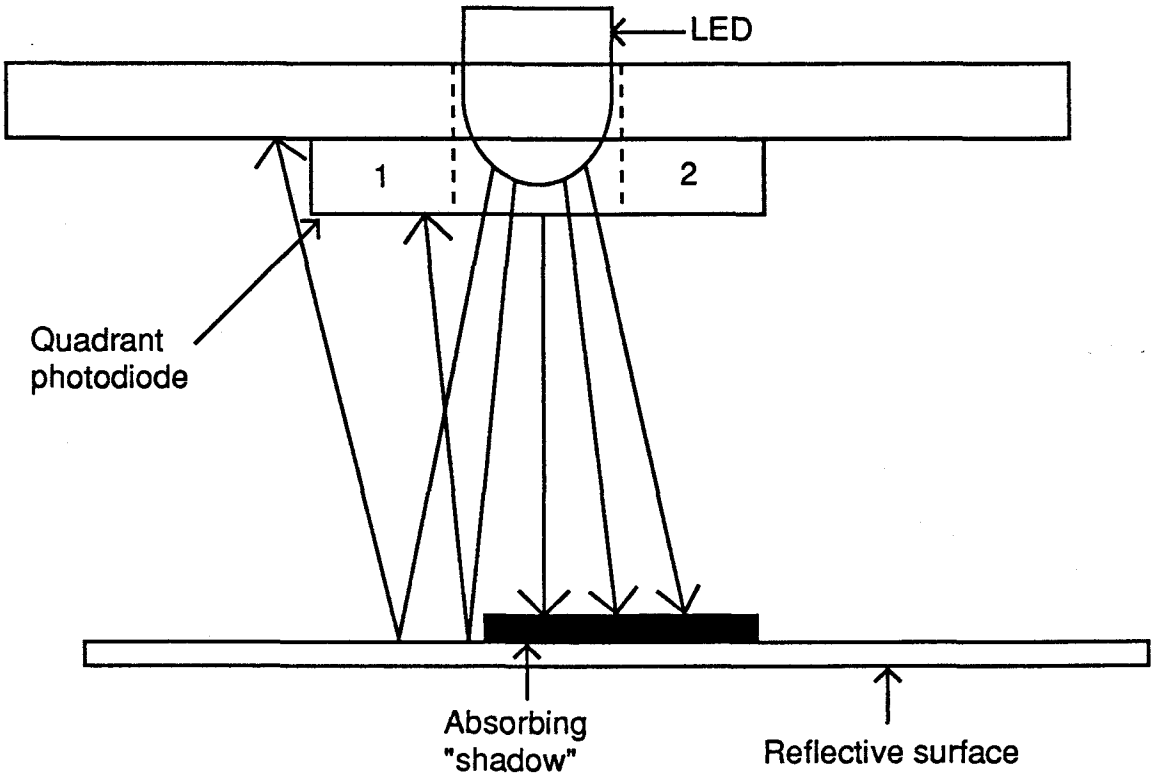
LED
1
2
Quadrant
photodiode
Absorbing
"shadow"
Reflective surface

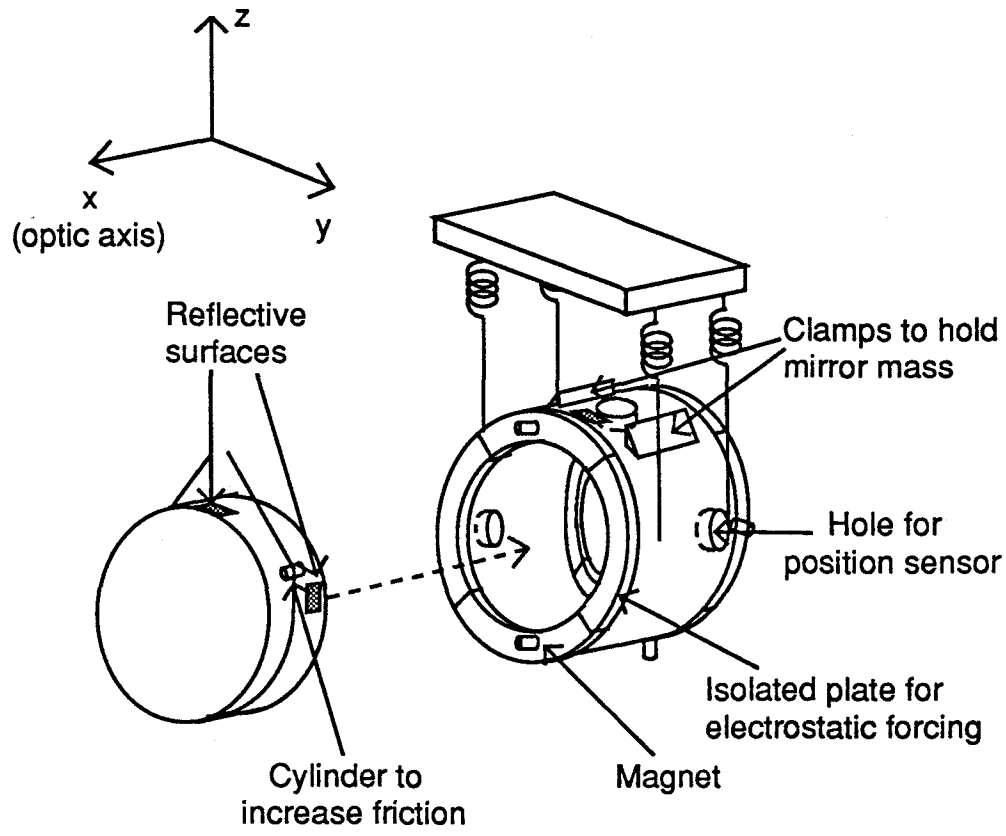
z
x
(optic axis)
y
Reflective
surfaces
Clamps to hold
mirror mass
Hole for
position sensor
Isolated plate for
electrostatic forcing
Cylinder to
increase friction
Magnet
Mirror mass
(hangs inside shell)
Shell

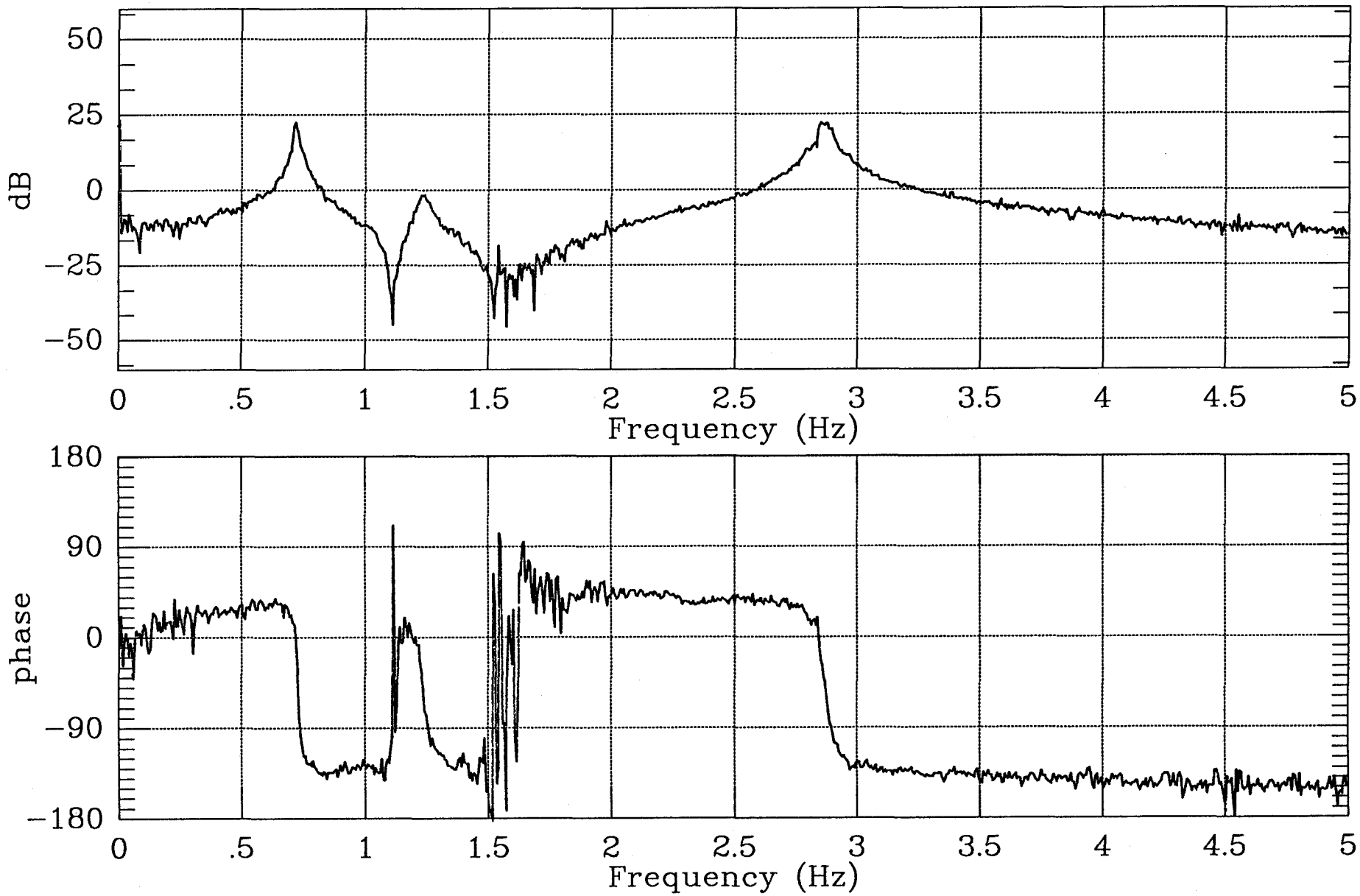
50
25
0
−25
−50
dB
0
.5
1
1.5
2
2.5
3
3.5
4
4.5
5
Frequency (Hz)
180
90
0
−90
−180
phase
0
.5
1
1.5
2
2.5
3
3.5
4
4.5
5
Frequency (Hz)

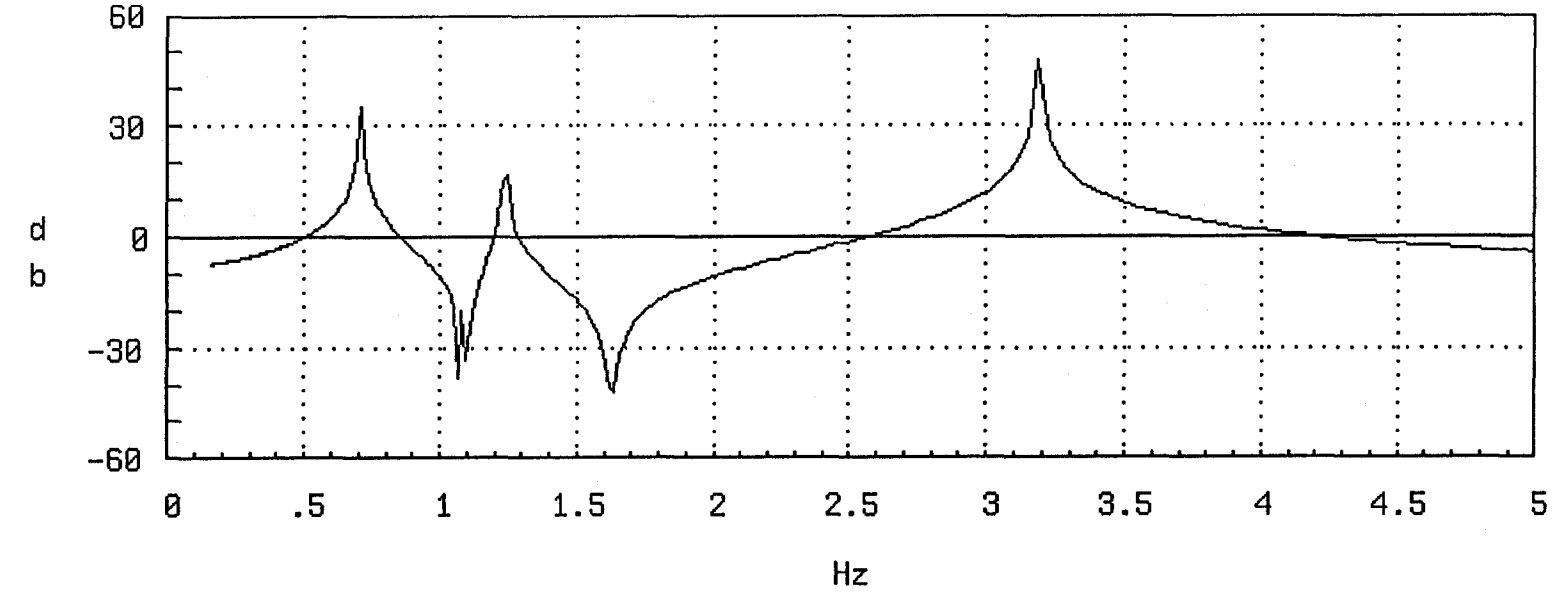
60
30
0
-30
-60
d
b
0
.5
1
1.5
2
2.5
3
3.5
4
4.5
5
Hz

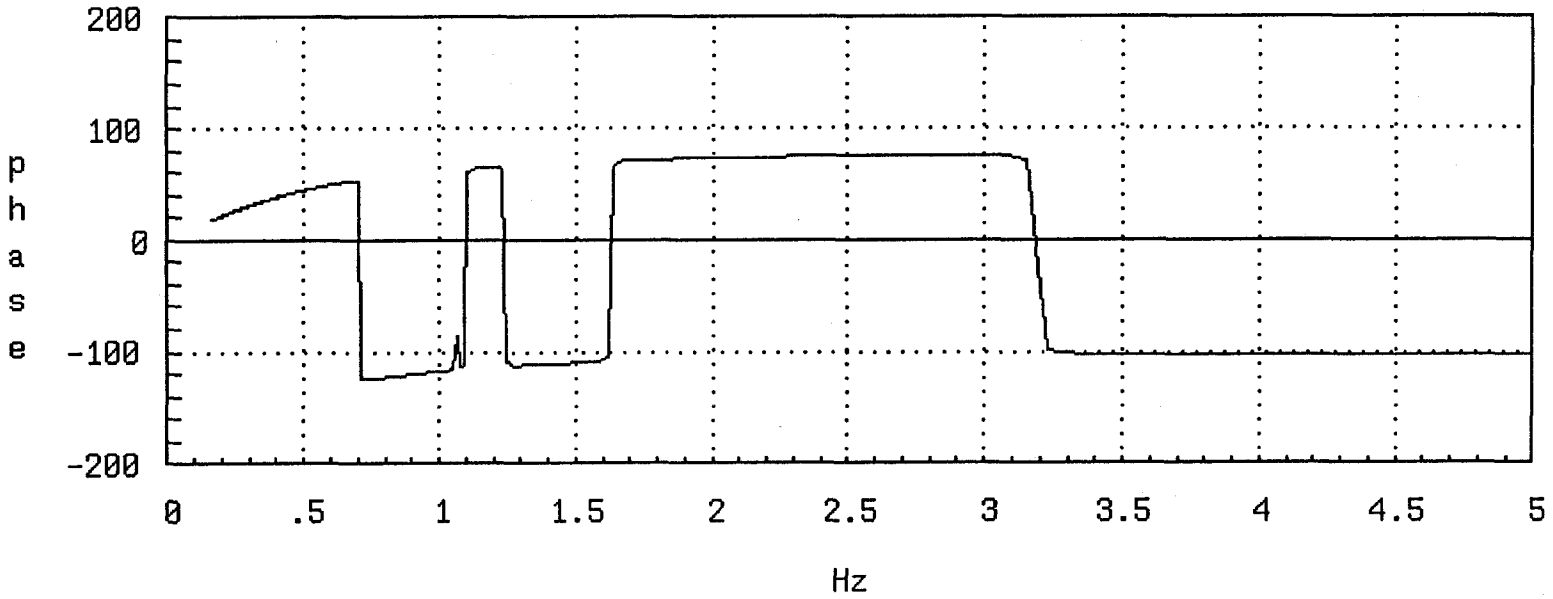
200
100
0
-100
-200
p
h
a
s
e
0
.5
1
1.5
2
2.5
3
3.5
4
4.5
5
Hz

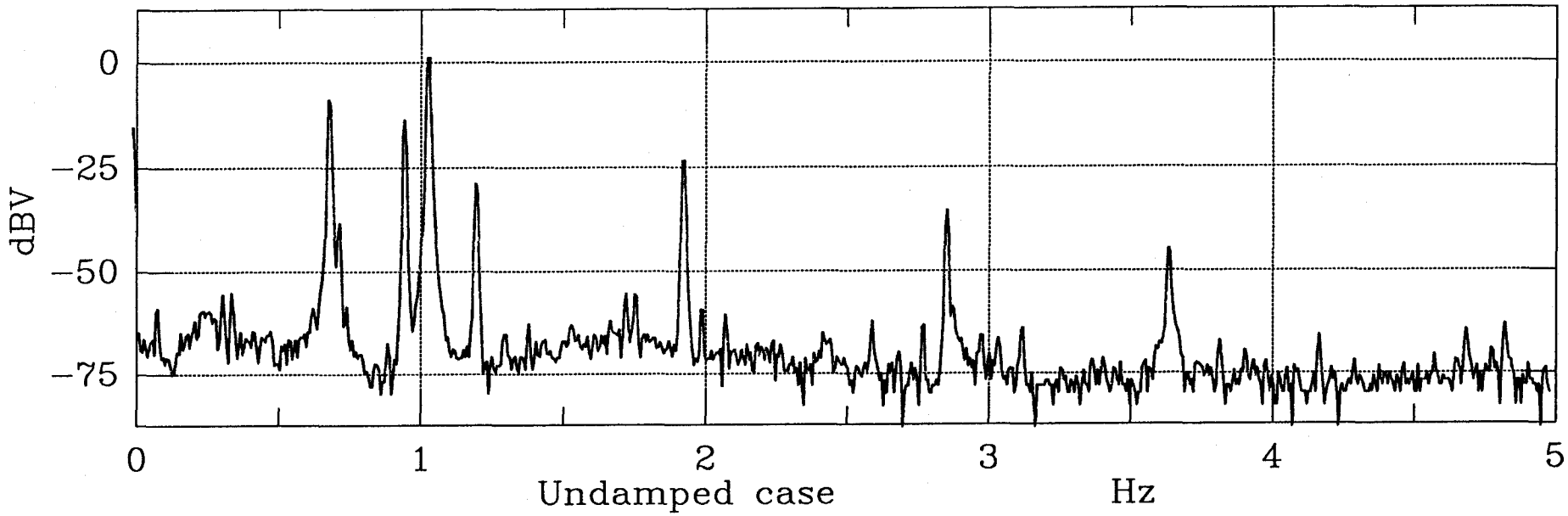
0
−25
−50
−75
dBV
0
1
2
3
4
5
Undamped case
Hz

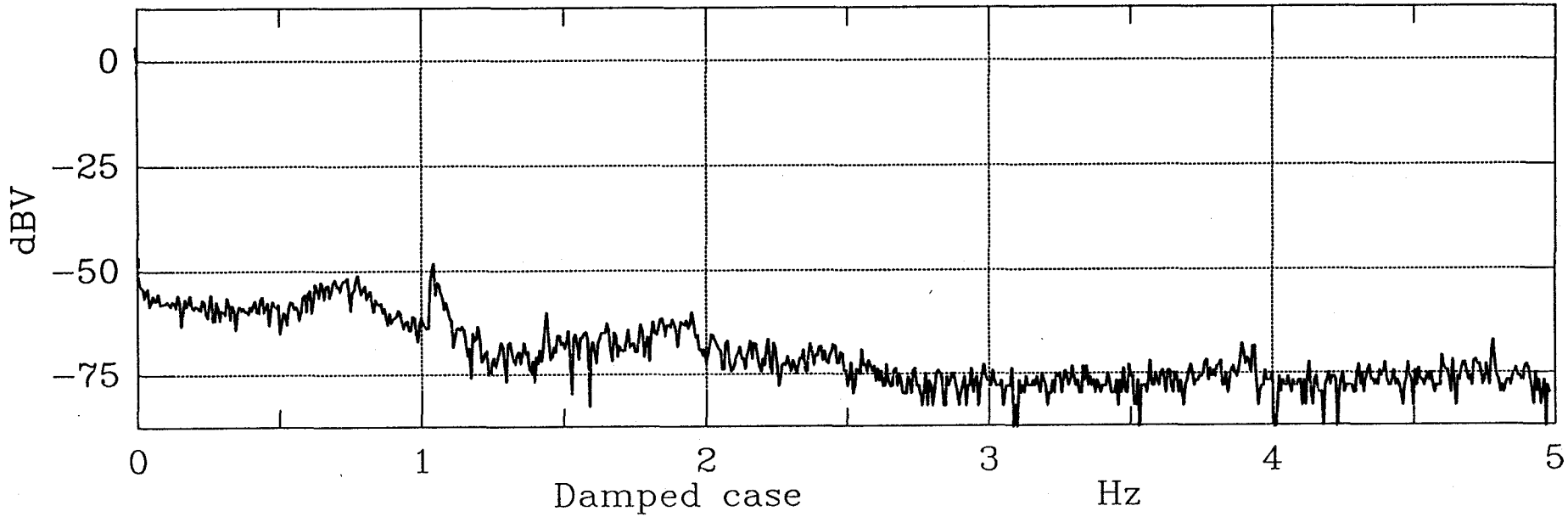
0
−25
−50
−75
dBV
0
1
2
3
4
5
Damped case
Hz

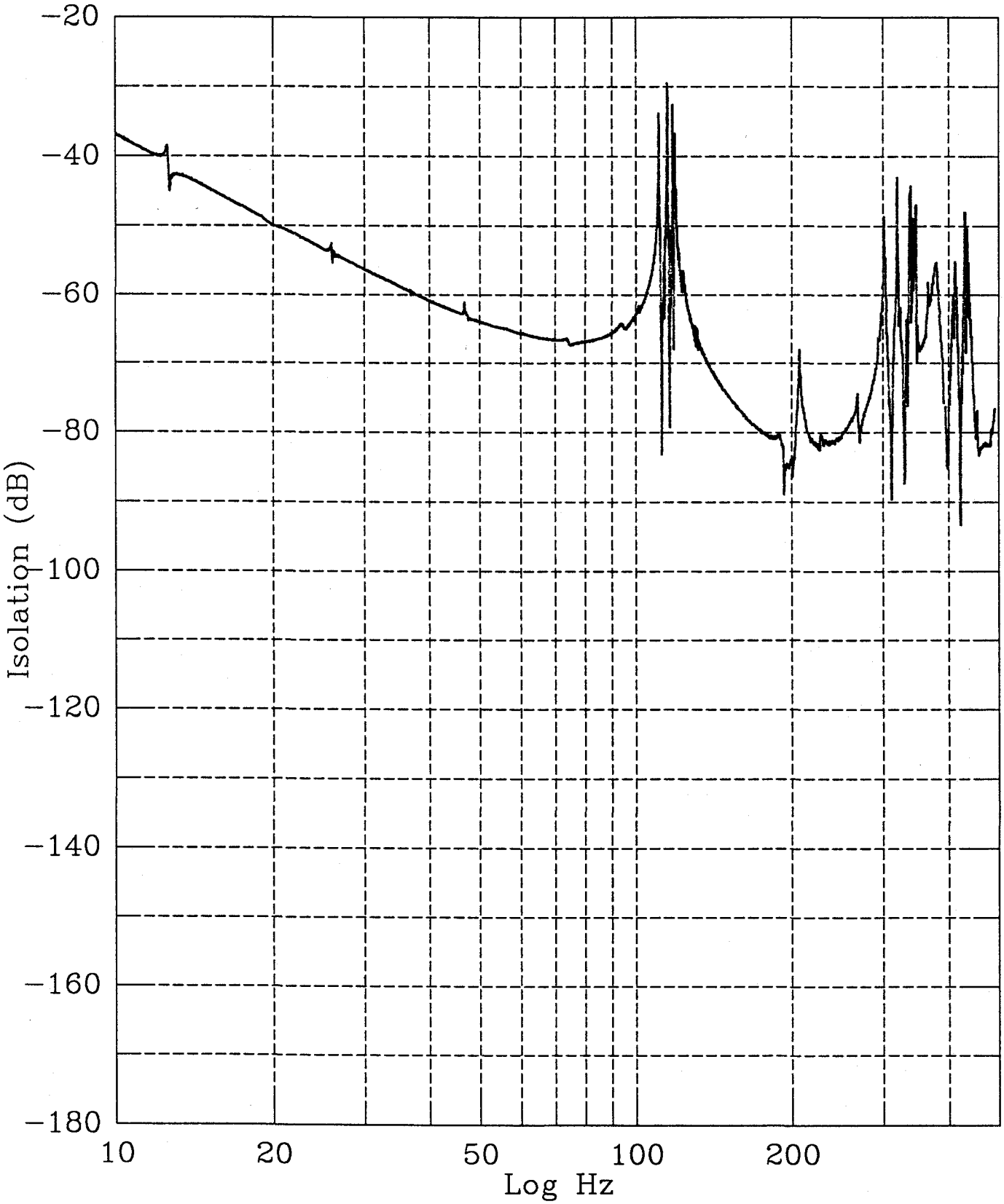
-20
-40
-60
-80
-100
-120
-140
-160
-180
Isolation (dB)
10
20
50
100
200
Log Hz

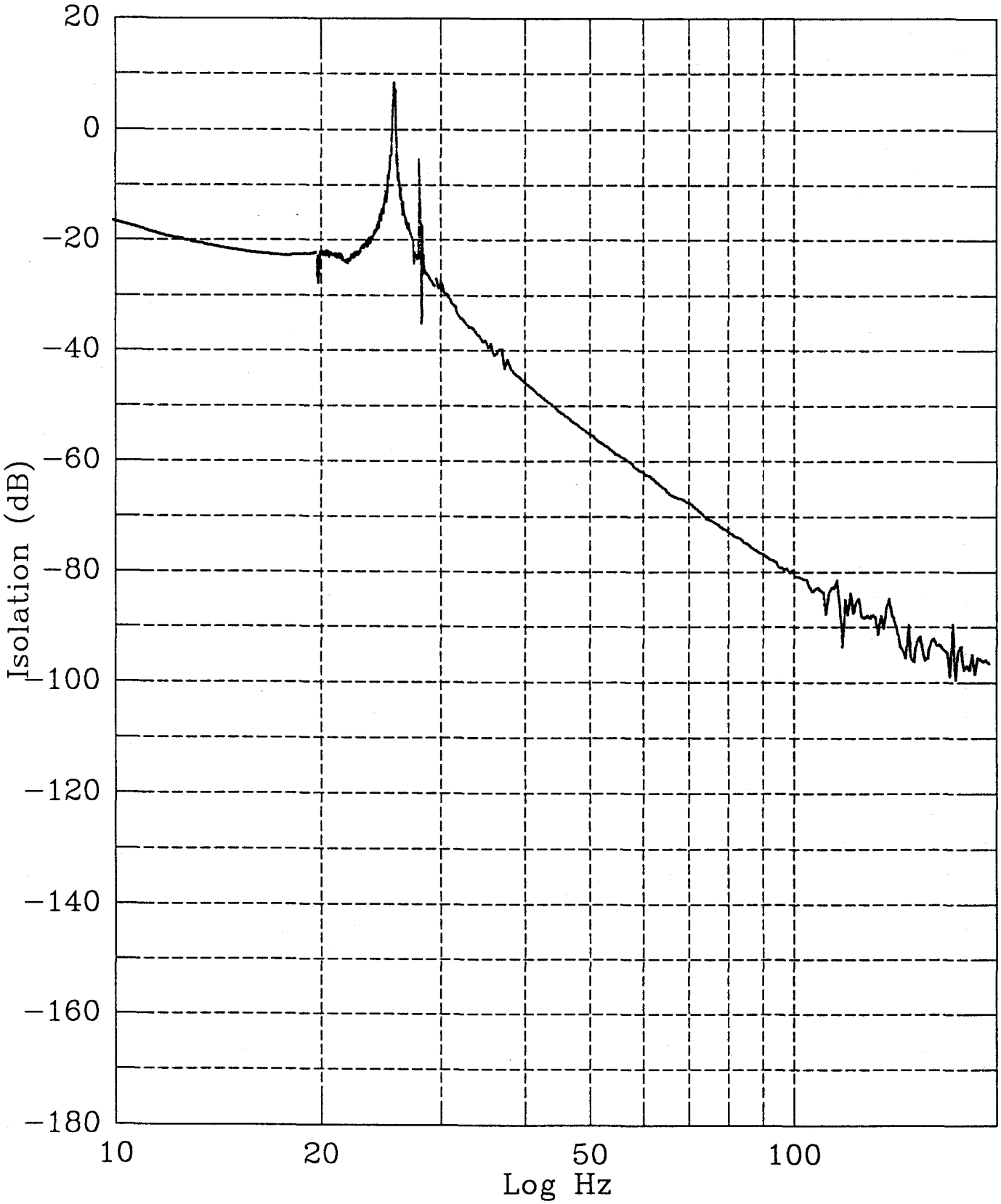
20
0
-20
-40
-60
-80
-100
-120
-140
-160
-180
Isolation (dB)
10
20
50
100
Log Hz

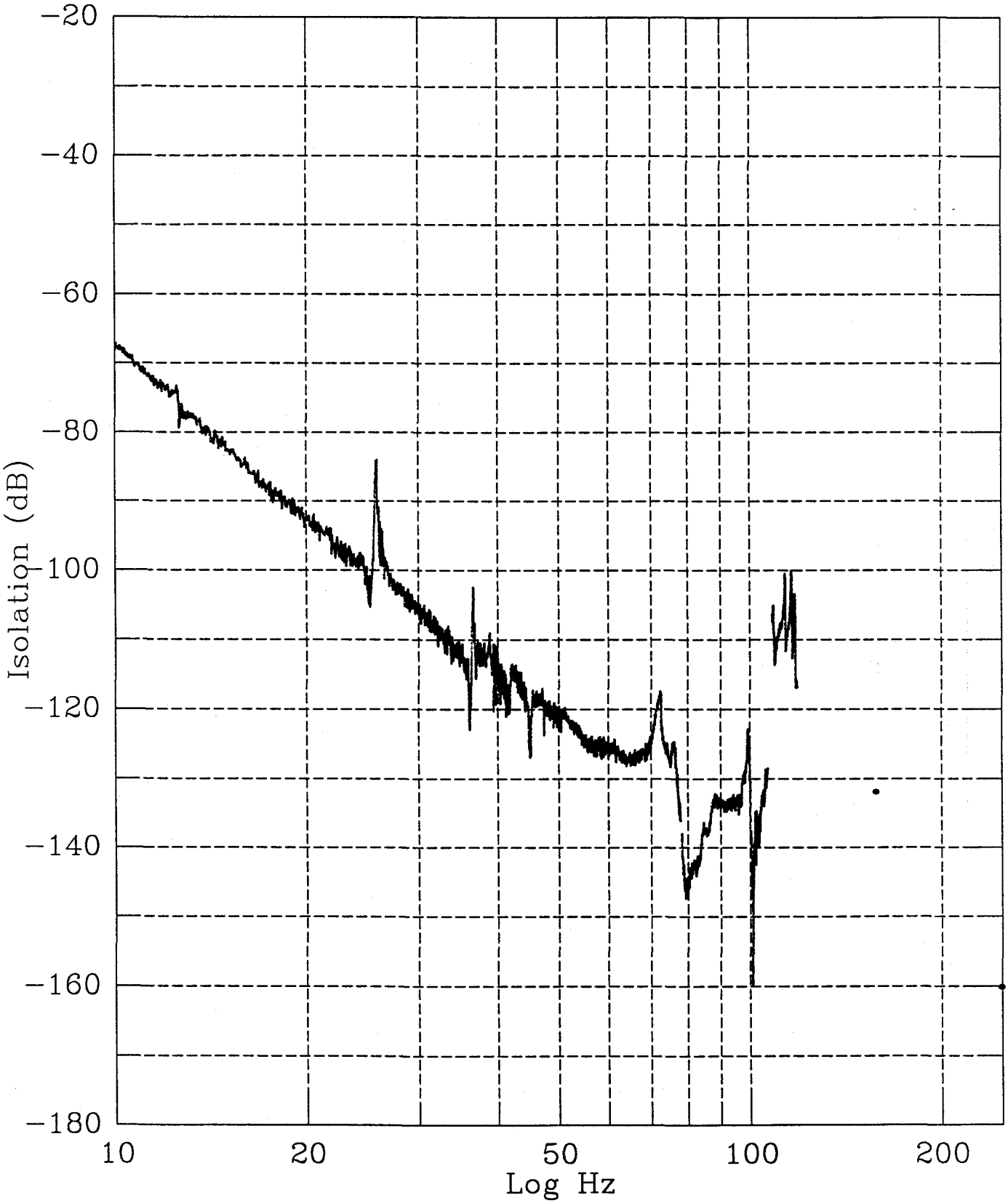
-20
-40
-60
-80
-100
-120
-140
-160
-180
Isolation (dB)
10
20
50
100
200
Log Hz

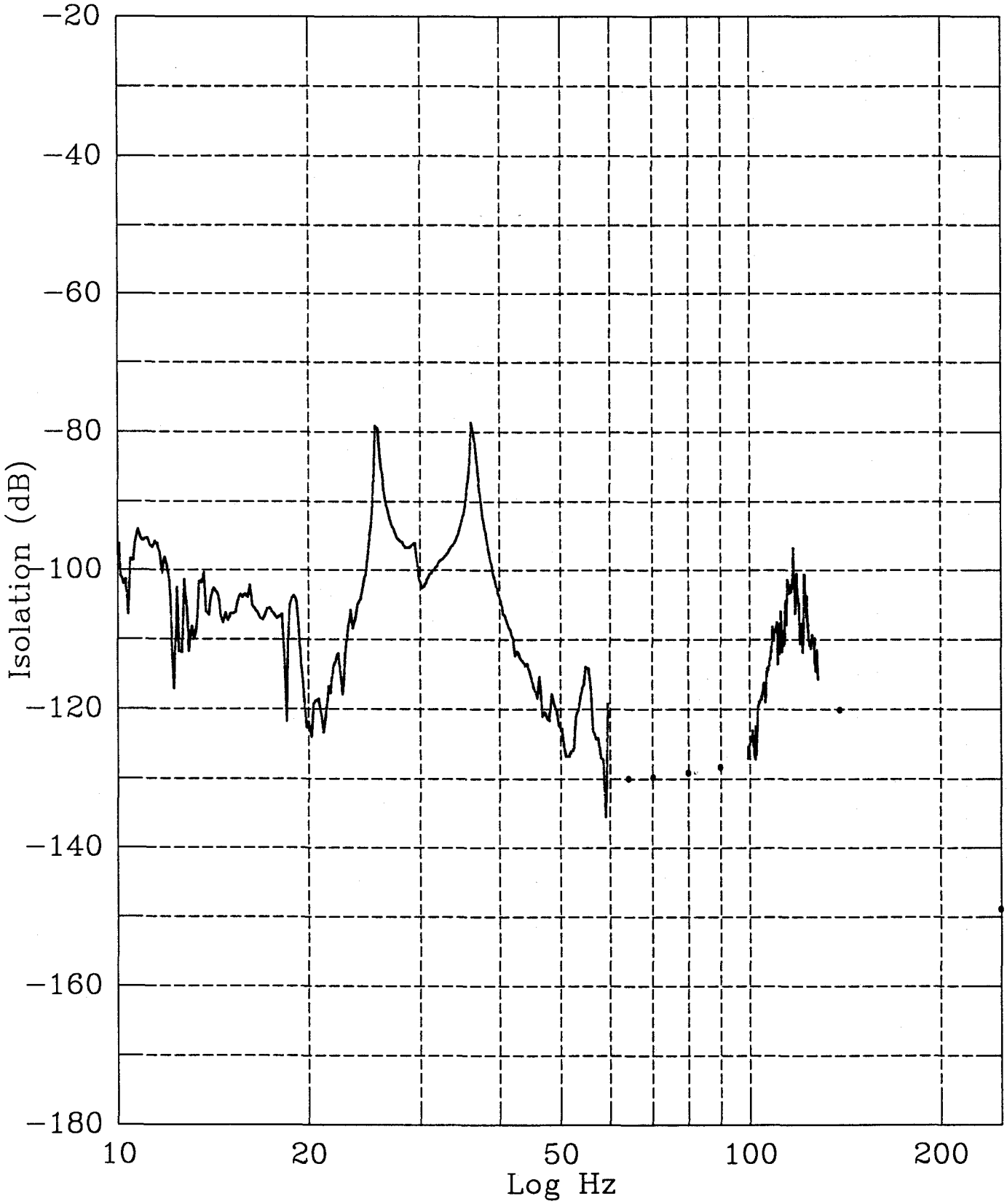
-20
-40
-60
-80
-100
-120
-140
-160
-180
Isolation (dB)
10
20
50
100
200
Log Hz

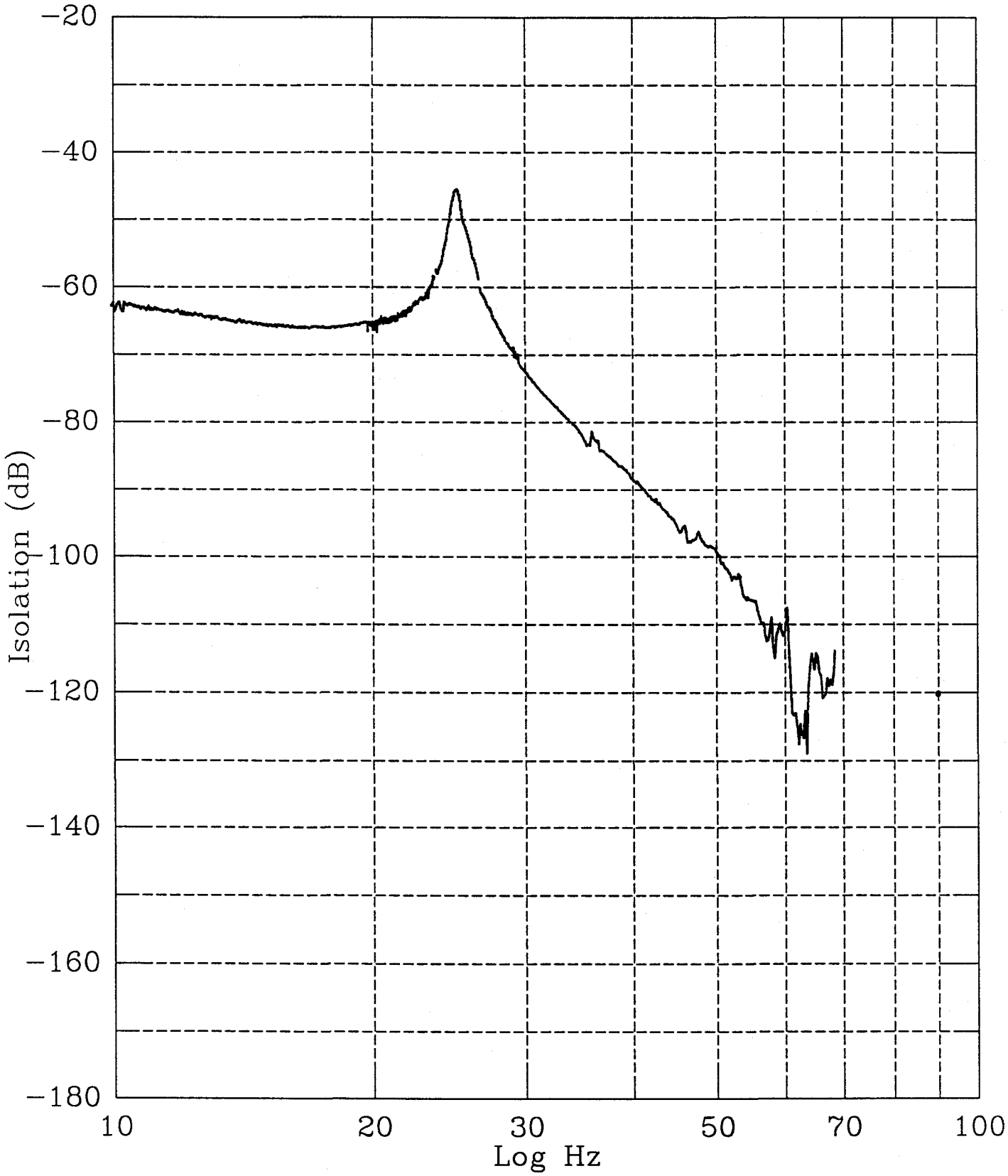
-20
-40
-60
-80
-100
-120
-140
-160
-180
Isolation (dB)
10
20
30
50
70
100
Log Hz

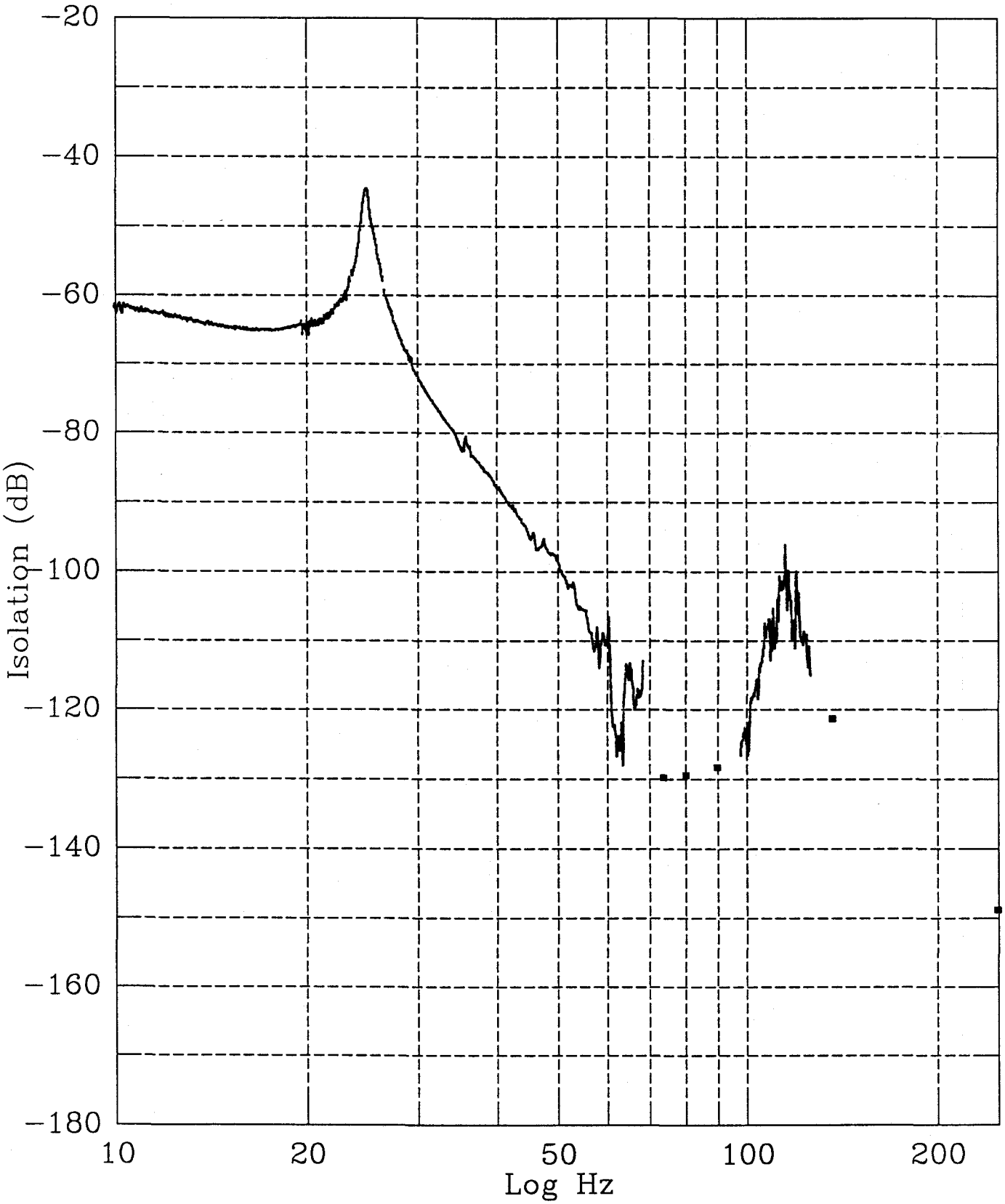
-20
-40
-60
-80
-100
-120
-140
-160
-180
Isolation (dB)
10
20
50
100
200
Log Hz

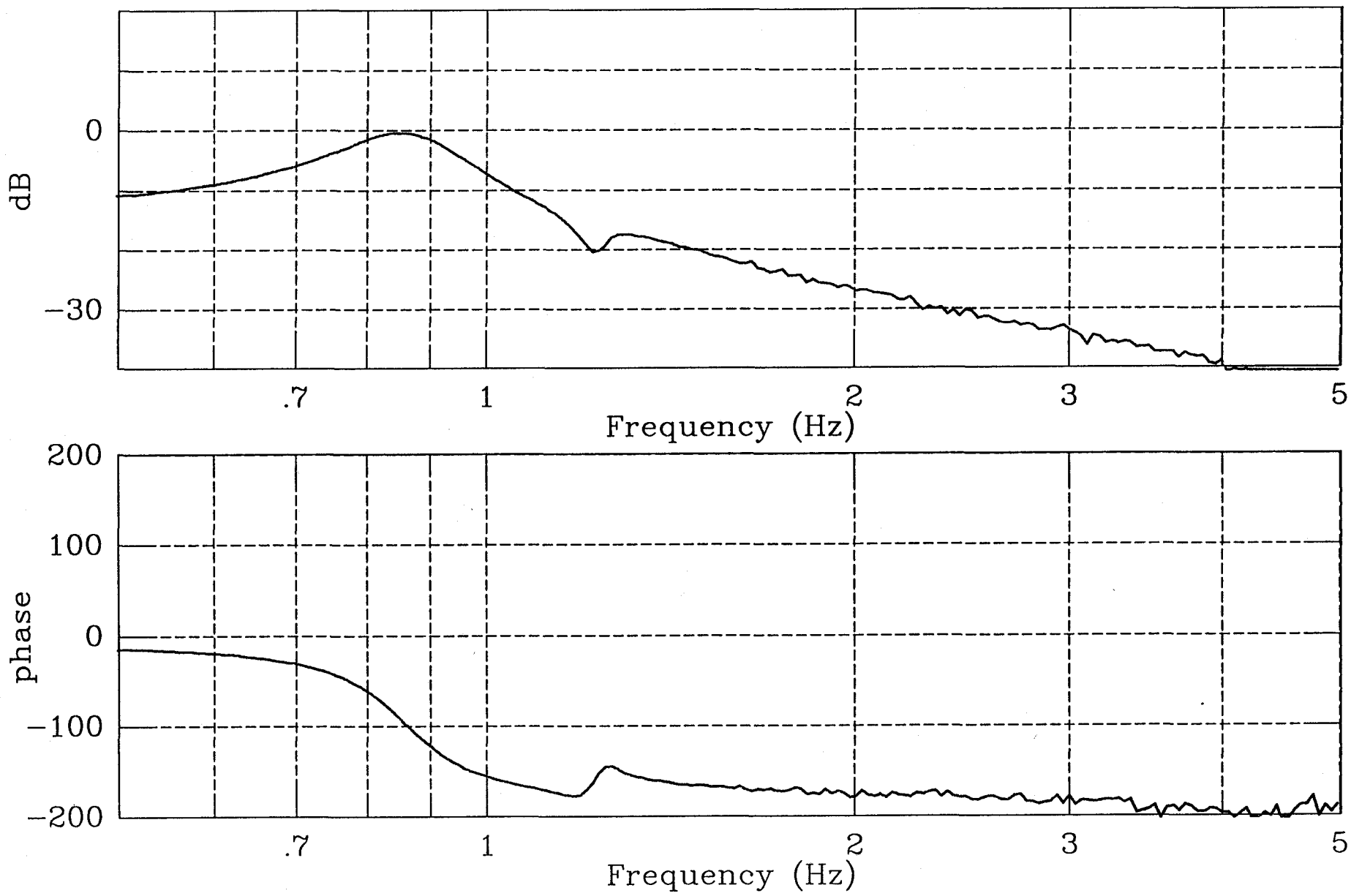
0
dB
−30
.7
1
2
3
5
Frequency (Hz)
200
100
0
phase
−100
−200
.7
1
2
3
5
Frequency (Hz)

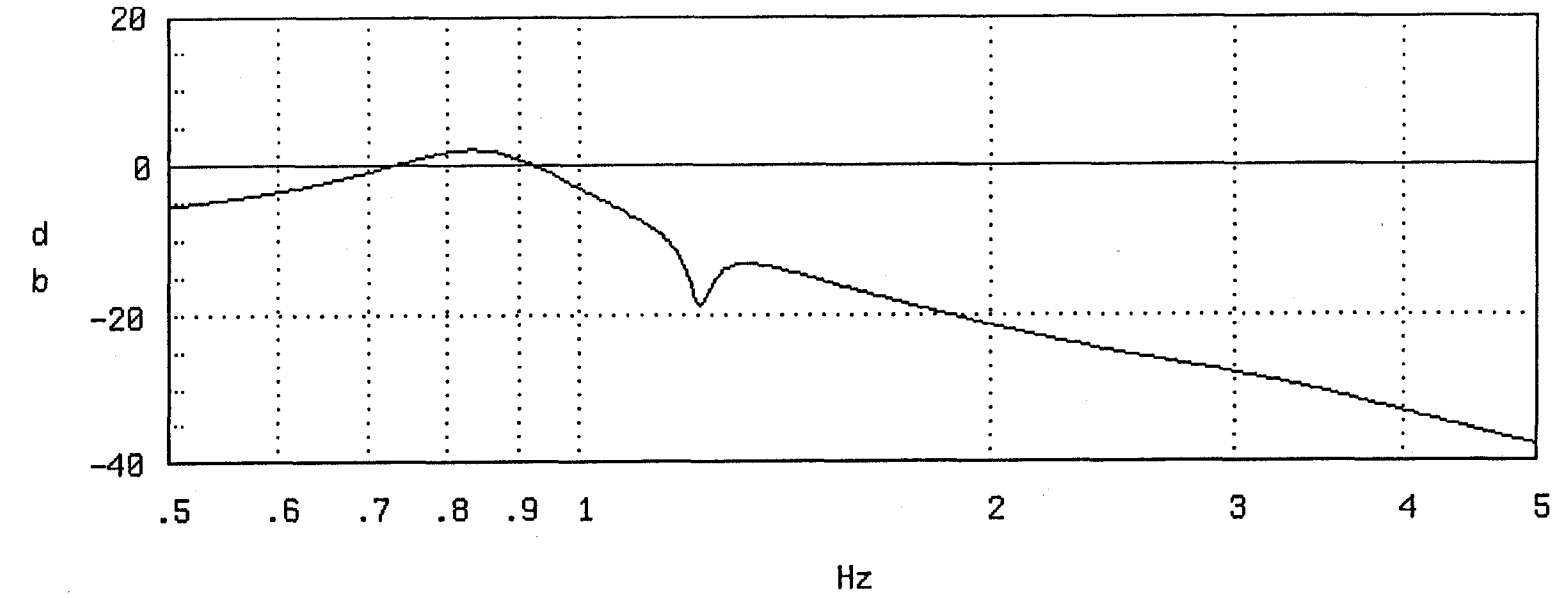
20
0
-20
-40
d
b
.5
.6
.7
.8
.9
1
2
3
4
5
Hz

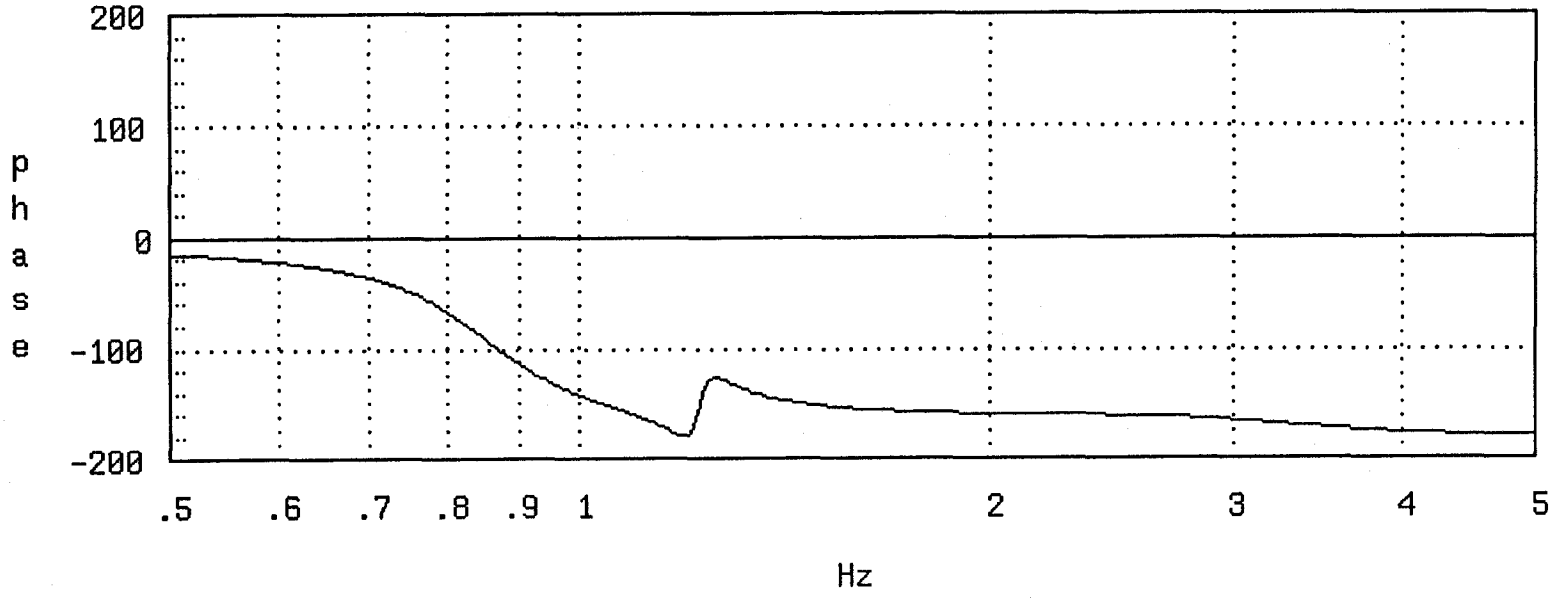
200
100
0
-100
-200
p
h
a
s
e
.5
.6
.7
.8
.9
1
2
3
4
5
Hz

11b

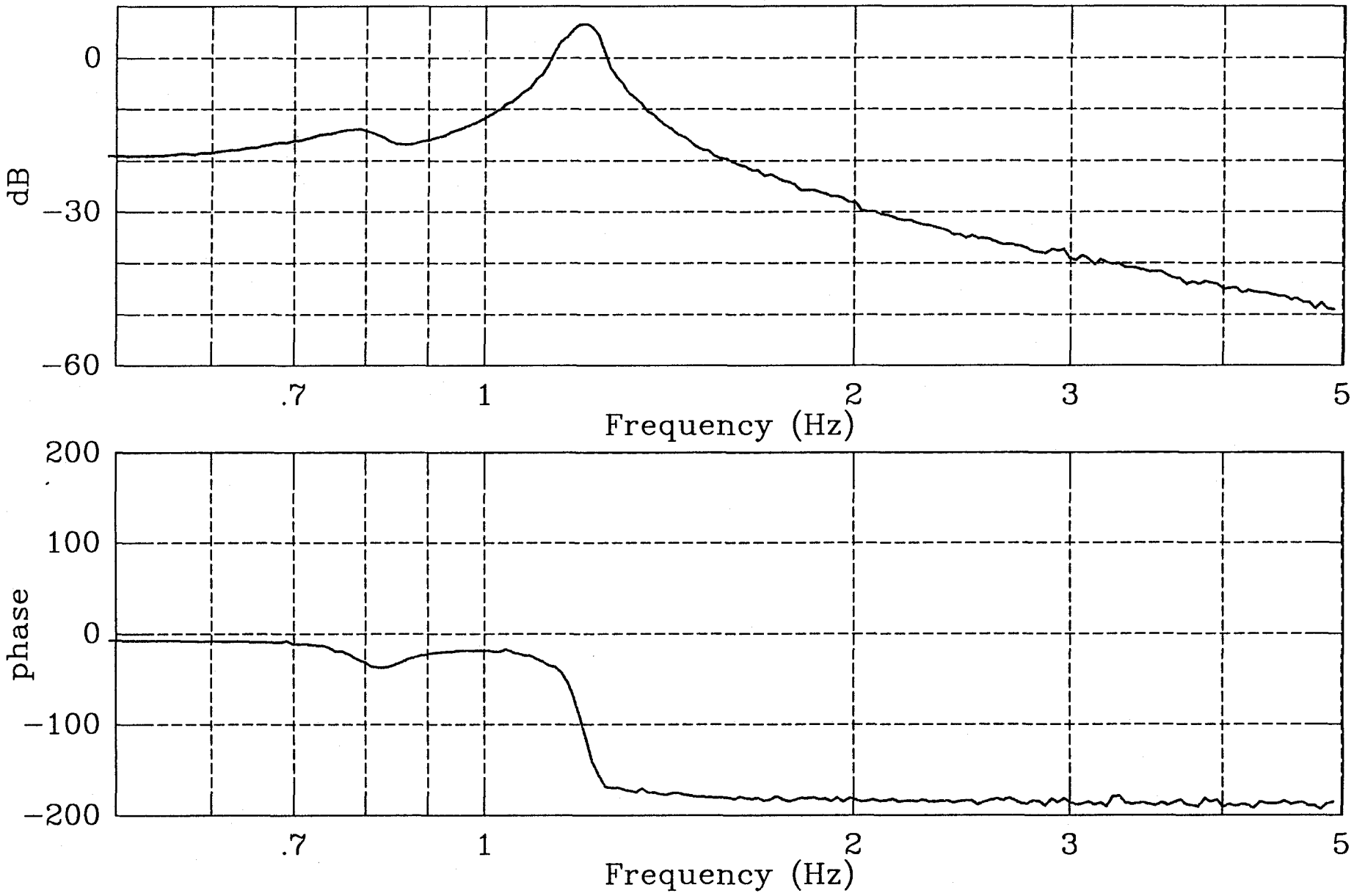
0
−30
−60
dB
.7
1
2
3
5
Frequency (Hz)
200
100
0
−100
−200
phase
.7
1
2
3
5
Frequency (Hz)

12a

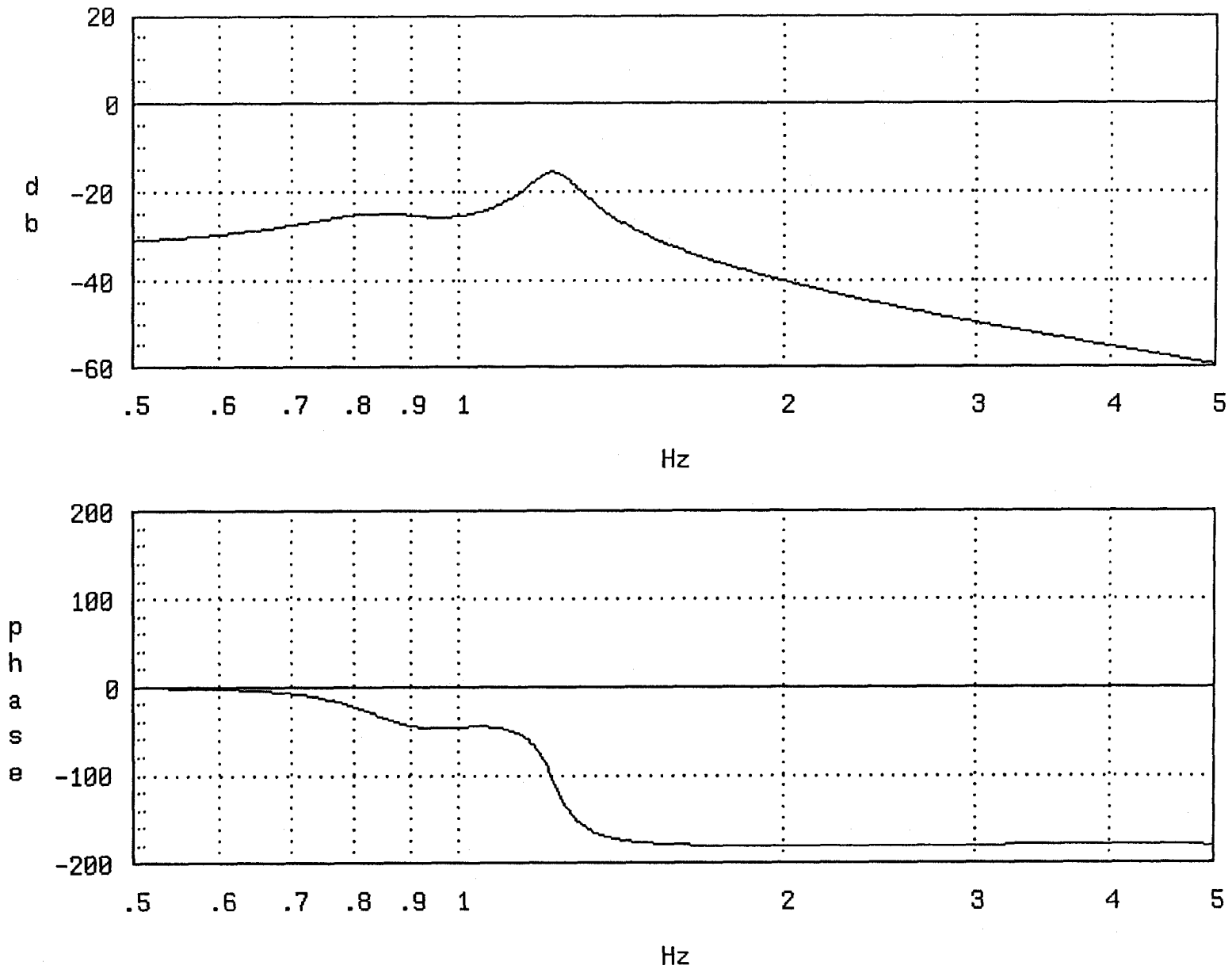
20
0
-20
-40
-60
d
b
.5
.6
.7
.8
.9
1
2
3
4
5
Hz
200
100
0
-100
-200
p
h
a
s
e
.5
.6
.7
.8
.9
1
2
3
4
5
Hz

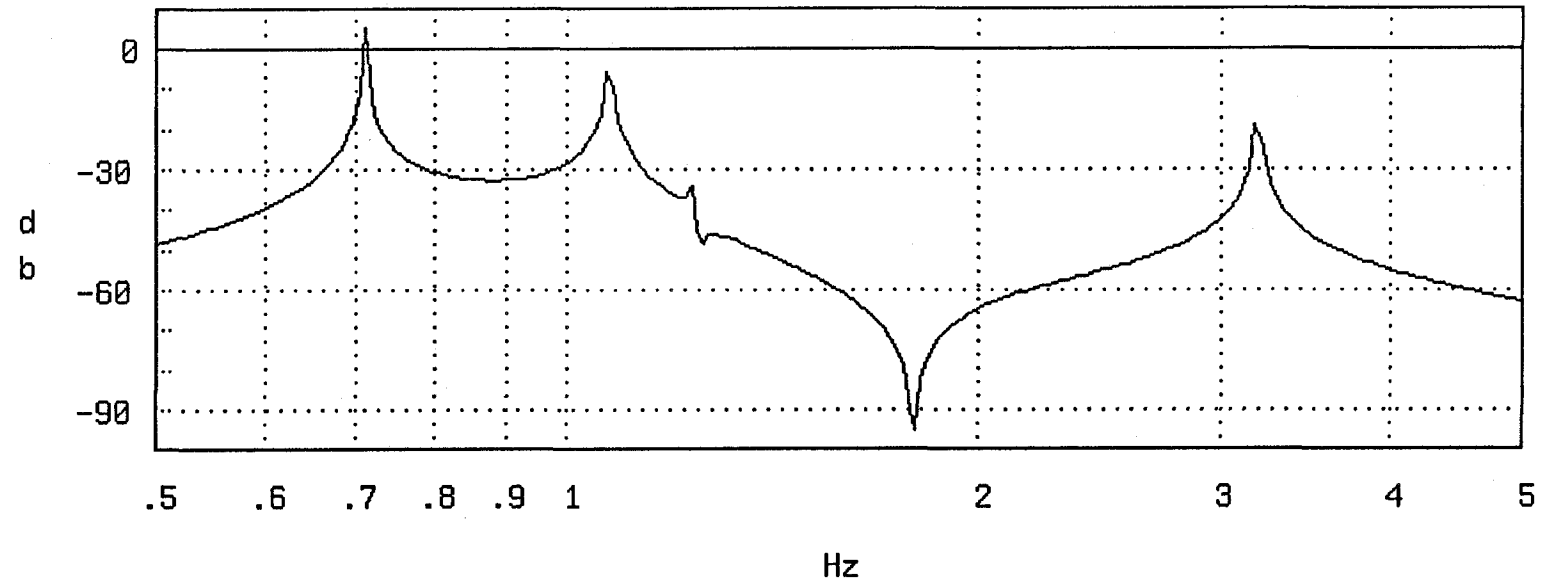
0
-30
-60
-90
d
b
.5
.6
.7
.8
.9
1
2
3
4
5
Hz

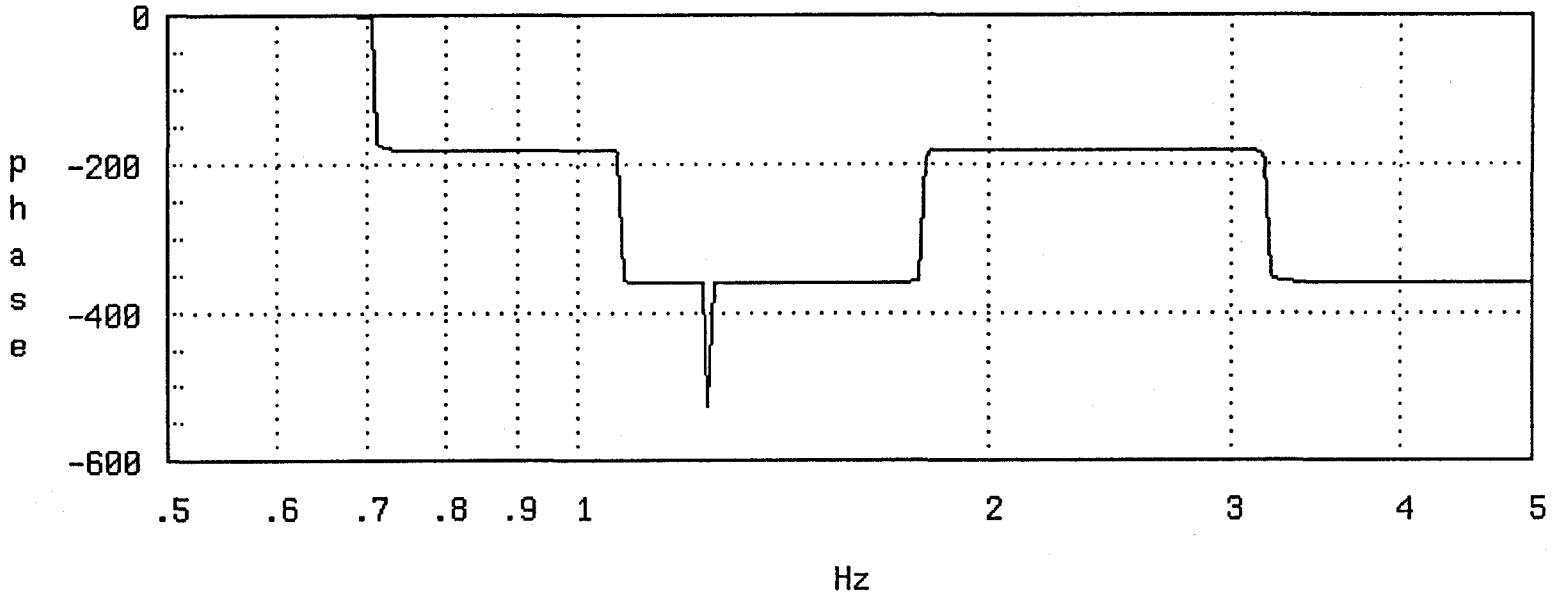
0
-200
-400
-600
p
h
a
s
e
.5
.6
.7
.8
.9
1
2
3
4
5
Hz